How Ocular Dominance and Binocularity Are Reflected by the Population Receptive Field Properties

Pieter B. de Best,[1] Noa Raz,[1] Serge O. Dumoulin,[2] and Netta Levin[1]

[1]fMRI lab, Neurology Department, Hadassah Hebrew University Medical Center Jerusalem, Israel
[2]Spinoza Centre for Neuroimaging, Amsterdam, The Netherlands

Correspondence: Netta Levin, fMRI Unit, Neurology Department, Hadassah Hebrew University Medical Center, POB 12,000, Jerusalem 91120, Israel;
netta@hadassah.org.il.

Submitted: March 5, 2018
Accepted: October 1, 2018

Citation: de Best PB, Raz N, Dumoulin S, Levin N. How ocular dominance and binocularity are reflected by the population receptive field properties. *Invest Ophthalmol Vis Sci*. 2018;59:5301–5311. https://doi.org/10.1167/iovs.18-24161

Purpose. The neural substrate of binocularity and sighting ocular dominance in humans is not clear. By utilizing the population receptive field (pRF) modeling technique, we explored whether these phenomena are associated with amplitude and pRF size differences.

Methods. The visual field maps of 13 subjects were scanned (3-T Skyra) while viewing drifting bar stimuli. Both eyes (binocular condition), the dominant eye and the nondominant eye (two monocular conditions) were stimulated in separate sessions. For each condition, pRF size and amplitude were assessed. Binocular summation ratios were calculated by dividing binocular by mean monocular values (amplitude and pRF size).

Results. No differences in pRF size were seen between the viewing conditions within each region, that is, either between binocular and monocular or between dominant and nondominant viewing conditions. Binocular amplitudes were higher than the monocular amplitudes, but similar among the dominant and nondominant eyes. Binocular summation ratios derived from amplitudes were significantly higher than one (~1.2), while those ratios derived from pRF size were not. These effects were found in all studied areas along the visual hierarchy, starting in V1.

Conclusions. Neither the amplitude nor the pRF size show intereye difference and therefore cannot explain the different roles of the dominant and the nondominant eyes. Binocular, as compared to monocular vision, resulted in higher amplitudes, while receptive fields' sizes were similar, suggesting increased binocular response intensity as the basis for the binocular summation phenomenon. Our results could be applicable in imaging studies of monocular disease and studies that deal with nondisparity binocularity effects.

Keywords: population receptive field, fMRI, binocular vision, binocular summation

Binocular vision is the blending of separate images seen by each eye into one composite image. This is advantageous from various perspectives, including a wider field of view, stereopsis, and reduction of detection threshold (as compared to monocular viewing), a phenomenon known as "binocular summation."[1–4] Reduced binocular summation was suggested to be the consequence of saturation of perception as in high contrasts and long stimulus durations.[1] Reduced binocular summation was also reported to be associated with increasing eccentricity.[2,5]

Binocular stimulation in cats and macaque monkeys resulted in a higher firing rate response in comparison to monocular stimulation and even caused the neuron to fire when monocular stimulation was insufficient to induce a response (subthreshold stimuli, reflecting binocular summation).[6–8] In humans, binocular summation was demonstrated in response to low contrast stimuli, as increased blood oxygenation level-dependent (BOLD) peak response during binocular versus monocular viewing condition. No binocular summation was evident for high contrast stimuli.[9]

"Ocular dominance" is the tendency to prefer visual input from one eye over the other. Controversy regarding the definition of ocular dominance exists in the literature, and different aspects of dominancy (such as better acuity and rivalry) are described (for a review, see Mapp et al.[10]). Sighting ocular dominance defines the dominant eye as the one that better describes the binocular vision. Different sighting eye dominance tests (among them, the Miles test) have high intercorrelation and test-retest reliability.[10,11] However, unlike handedness, this preference is subtle and subjects are frequently unaware of it.[12] Ocular dominance, as defined by increased firing rates in response to stimulation of the preferred eye, has been demonstrated in cats and macaque monkeys.[7,13] Other measurements, including receptive field (RF) shape, axis orientation, and excitatory/inhibitory configuration were not associated with ocular dominance.[7,8,13] Studies in humans using functional magnetic resonance imaging (fMRI) demonstrated larger activation areas in response to stimulation of the sighting-dominant eye[14] but similar percent signal change.[15,16]

Our visual world contains features with a wide range of object scales, such as different spatial frequencies, and can be considered as broadband. In contrast, single neurons in V1 are narrowband, that is, narrowly tuned to specific spatial scales. Thus, to perceive the broadband picture, the narrowband information from single neurons requires integration. This integrational process is highly relevant to ocular dominance and binocular processing.[17]

In the current study, we aimed to investigate the neural substrate of binocularity and ocular dominance in humans, using the population receptive field (pRF) modeling tech-

nique.[18] Utilizing the advantage of this technique, our study explored whether ocular dominance and binocular summation are associated with differences in amplitude and pRF size.

We evaluated two potential hypotheses:

H1: Behavioral functioning may be explained by pRF size. Smaller receptive field sizes are associated with improved visual acuity,[19–23] so we expect that binocular pRF sizes will be smaller than the monocular ones, and within the monocular stimuli, the dominant eye will produce smaller pRF sizes.

H2: The second hypothesis relates behavioral functioning to response amplitude, suggesting increased BOLD amplitude in binocular versus monocular stimulations, as well as during dominant versus nondominant ones.

Methods

Subjects

We examined 13 normal sighted subjects, all had 20/30 or better corrected visual acuity. The study group included 9 females, median age 25.4 years (range, 22–43). Nine participants were right eye dominant, according to the Miles test.[15,24] Hadassah Hebrew University Medical Center Ethics Committee approved the experimental procedure based on the tenets of the Declaration of Helsinki; written informed consent was obtained from all subjects after explanation of the nature and possible consequences of the study.

Study Design

Drifting bar stimuli (as described in Klein et al.[25] and Zuiderbaan et al.[26]) were used in three different viewing conditions: binocular, monocular-dominant, and monocular-nondominant (see Fig. 1A). For the monocular conditions, a patch was used to cover one eye. For each viewing condition, stimuli runs were repeated four times. Participants were asked to switch patches after the fourth run of each viewing condition with the aim of limiting movement. Inplane scans (see "MRI Data Acquisition") were performed following the patch switch, and functional data were co-registered to the anatomical scan to avoid bias from any remaining inter-viewing condition movements. Viewing condition order was counterbalanced across participants.

In each run, a 2° bar aperture, occurring in four possible orientations—horizontal, vertical, and two diagonals—drifted through the visual field in eight directions perpendicular to bar orientation. The bar aperture moved in 16 steps of 1° and 1.5 seconds through the display. A circular checkerboard display (16° diameter,) was seen through this moving bar aperture. Thus, stimuli length was defined by its current orientation and position within the display (Fig. 1A). The checkerboard spatial fundamental frequency was 0.5 cycles per degree, and the checkers moved in opposite directions parallel to bar orientation, switching direction after 4 seconds or more.

To control for fixation, a central task requiring the participants to report color changing of a fixation dot was administered. After each horizontal or vertical bar pass, there was a 12-second baseline period in which the participant was presented only with a fixation dot, and continued fixation (Fig. 1A).

Stimuli were created in Matlab using the VISTADISP toolbox (https://github.com/vistalab/vistadisp, available in the public domain) and Psychtoolbox.[27] Stimuli were transferred through a mirror converter box to a 32″ MR-compatible LCD Monitor (NordicNeuroLab, Bergen, Norway), which was placed at a 140-cm viewing distance. The stimuli were projected onto a mirror above the face of the participant.

MRI Data Acquisition

Scans were performed using a 3T Siemens MAGNETOM Skyra scanner (Siemens Healthcare GmbH, Erlangen, Germany).

To acquire 20 coronal functional slices covering the visual areas, the posterior part of the 32-channel receiver coil was used to perform 2D echo-planar imaging sequences (repetition time (TR)/echo time (TE) 1500/27 ms, flip angle 55°, isotropic voxel size 2.5 mm, field of view = 180 × 180 mm). Inplane anatomical scans (TR/TE 300/3.78 ms, flip angle 60°, voxel size 0.8 × 0.8 × 2.5 mm, 20 coronal 200 × 200 mm slices) were performed after each viewing condition. The full 32-channel coil was used to perform a high-quality magnetization-prepared rapid acquisition with gradient echo (MPRAGE; TR/TE 2300/2.98 ms, flip angle 9°, isotropic voxel size 1 mm, 160 axial 256 × 256 mm slices covering the whole brain).

Data Analysis

Using the VISTASOFT toolbox (https://github.com/vistalab/vistasoft, available in the public domain), functional scans were preprocessed. This encompassed removal of eight pre-scan volumes, slice timing correction, and rigid-body motion compensation, including between scans and within scan alignment (using code originally described by Nestares and Heeger[28]). The high-quality anatomical scans were realigned in AC (anterior commissure)-PC (posterior commissure) space by identifying the anterior and posterior commissure. Subsequently, gray-white matter segmentation was performed in FreeSurfer.[29]

After a first manual co-registration, the Nestares alignment,[28] SPM mutual information (http://www.fil.ion.ucl.ac.uk/spm/software/spm8/, available in the public domain) and, if necessary, the Kendrick Kay codes (https://github.com/kendrickkay/, available in the public domain) were used to automatically align the inplane to the anatomical scan. The resulting alignment was carefully inspected visually and, if required, edited manually.

Using the VISTASOFT toolbox, the pRF was modeled for all voxels that were part of a 3-mm gray matter layer, which was grown on the white matter surface. The pRF model, which describes the receptive field of the neural populations in each voxel, has been comprehensively described by Dumoulin and Wandell.[18]

The mrMesh subfunctionality of the VISTASOFT toolbox was used to generate and smooth 3D meshes of the gray matter brain surface. Eccentricity and polar angle values were calculated from the modeled pRF center, and polar angle reversals and eccentricity maps were used to delineate the visual brain areas V1, V2, V3, hV4, and TO1/TO2 (equivalent to MT+; see, for instance, Amano et al.[30] and Witthoft et al.[31]). An example of a delineation of the visual areas on the polar angle and eccentricity maps can be found in Figure 1B.

Statistical Analysis

BSDA, WRS, and WRS2 packages in R were used for statistical testing.

For assessment of the modeled pRF size (σ; defined here as the standard deviation of the best-fitting 2D Gaussian model), only voxels with variance explained (VE) >30% were included for further analysis,[19,32] but for assessment of amplitude, all voxels were included since preselecting on VE may bias the data toward higher data-derived % signal change amplitudes (β).

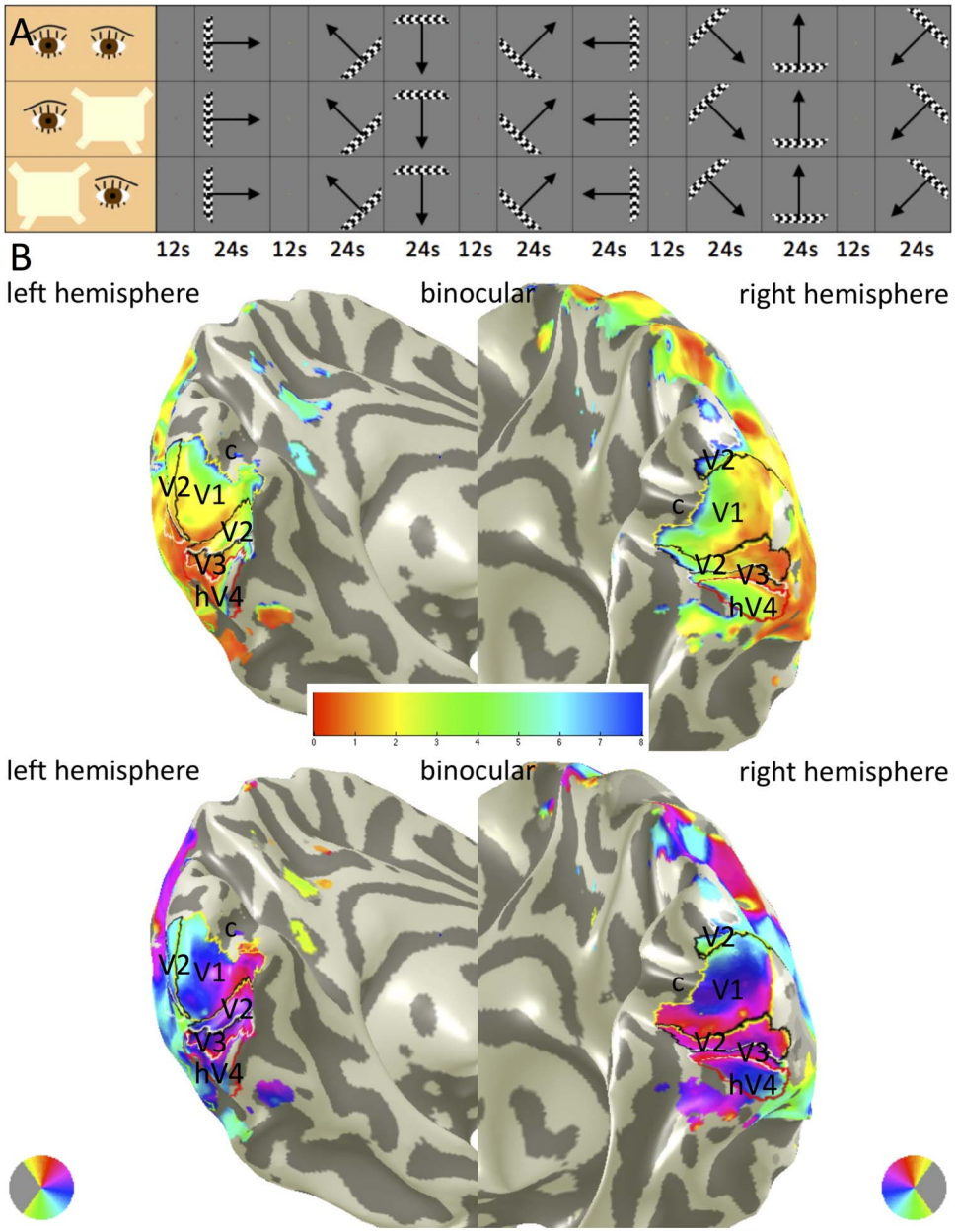

Figure 1. Study design, eccentricity and polar angle maps. (**A**) Design: participants view the stimuli with both eyes (*upper row*), right eye (*middle row*), and left eye (*lower row*). The session started with a 12-second mean luminance screen. Then 2° wide bars drifted through the screen in eight cardinal and orthogonal directions, exposing an 8° radius moving checkerboard. After each cardinal pass, there was a 12-second mean-luminance baseline period. (**B**) Eccentricity (*top*) and polar angle (*bottom*) maps: these images illustrate the eccentricity and polar angle maps in one of our participants (subject 9; according to the order used in Supplementary Fig. S1), mapped on the 3-dimentional surface of the individual brain. *Color bars*, and *circle diagrams* depict the represented eccentricities and polar angles, respectively. The calcarine sulcus is marked with a "c." For visualization purposes only, these maps were limited to variance explained (VE) > 0.01% and eccentricities from 0° to 8°.

Assuming that there is a linear relationship between σ (or β) and eccentricity, the fit of the baseline representing this relationship at 4°, represents, in a way, the average σ (or β) of all eccentricities in each ROI, to which all eccentricities contribute equally. Simply taking the average of the whole area would result in a stronger influence of low eccentricities relative to high eccentricities. Thus, for statistical analysis, individual σs and βs at 4° eccentricity were derived. In addition, to assess possible inconsistencies across eccentricities, σs and βs were assessed in clinical foveal (0.5°–2.5°), foveal/central (2.5°–5°), and parafoveal/paracentral (5°–7.5°) eccentricity ranges.

A mixed-model analysis of variance (ANOVA) with viewing condition (binocular, dominant, and nondominant eye) as within-subjects factor and condition order (binocular first or last) as between-subjects factor was performed on σ and β. Sphericity was evaluated and in cases where sphericity was violated, the sphericity-corrected P value was assessed. Assumptions of normality and equality of variance were assessed using the Shapiro-Wilk and Levene's homogeneity of variance tests, respectively. If these tests indicated assumption violations, either through significant ($P < 0.05$) or marginally significant ($P < 0.1$) results, the median was assessed with the robust version of the mixed model ANOVA

with 1000 bootstrap samples (https://CRAN.R-project.org/package=WRS2; see Field et al.,[33] Mair and Wilcox,[34] and Wilcox[35]). Results were Bonferroni multiple comparisons corrected for 5 comparisons in assessing at 4° (5 visual areas) and 15 comparisons in assessing in the 3 eccentricity ranges (5 visual areas * 3 eccentricity bins). A strict Bonferroni correction for multiple comparisons was used. Significant results that did not pass this strict correction are mentioned when relevant. If results were significant after multiple comparisons correction, paired *t*-tests or robust post hoc tests[36] were performed, depending on normality and homogeneity of variance assumptions, which were then Bonferroni corrected for three among-conditions comparisons.

"Binocular summation ratios" were defined as the binocular/averaged monocular values, derived from the fitted σ and β at 4°. This was separately calculated for the pRF size and percent signal change (BOLD amplitude) measures. The sign test or *t*-test were used (https://CRAN.R-project.org/package=BSDA, available in the public domain) depending on whether parametric assumptions were violated or not, to compare resulting summation ratios to 1 (ratios of 1 imply zero summation, as they result from equal binocular and average monocular values). Summation ratios were assessed at 4°, and at clinical foveal (0.5°–2.5°), central (2.5°–5°), and paracentral (5°–7.5°) eccentricity ranges. Bonferroni was then used to correct for, respectively, 5 and 15 comparisons. Significant results without multiple comparisons correction were also reported.

Results

Participants performed well on the fixation task in all conditions (>85%). No significant differences in fixation performance between conditions were detected.

Population Receptive Field Size (pRF)

Polar angle and eccentricity maps were typically distributed over the cortical surface, allowing delineation of V1, V2, V3, hV4, and TO1,2 (Figs. 1B, 2A, 2B). As expected, pRF size increased with eccentricity (Fig. 2C, 2D) and along the hierarchy (Fig. 2D).

At 4° (representing the visual area average), no differences were seen between the viewing conditions within each region, that is, neither between binocular and monocular nor between dominant and nondominant viewing conditions (Fig. 3A). However, when we separately examined the effects at the different eccentricities, higher pRF size for binocular than for nondominant eye viewing was seen at V2 at 5° to 7.5° (Fig. 3B).

Signal Amplitude

BOLD amplitudes seemed to increase with eccentricity (Fig. 4A) and decrease along the hierarchy (Fig. 4B). Binocular amplitudes were higher than the monocular amplitudes but similar between dominant and nondominant eyes (Fig. 4A, 4B).

At 4°, the main effects of viewing condition on amplitude were seen in all studied visual areas except TO1/TO2 (which was significant but did not pass correction for multiple comparisons). Post hoc tests revealed effects for the binocular-dominant contrast in V2, V3, and hV4, and for the binocular-nondominant contrast in V1 to V3, indicating that binocular amplitudes were significantly higher than monocular ones. Higher binocular amplitudes for the binocular-dominant contrast in V1 and the binocular-nondominant contrast in hV4 were also found but did not pass correction for multiple

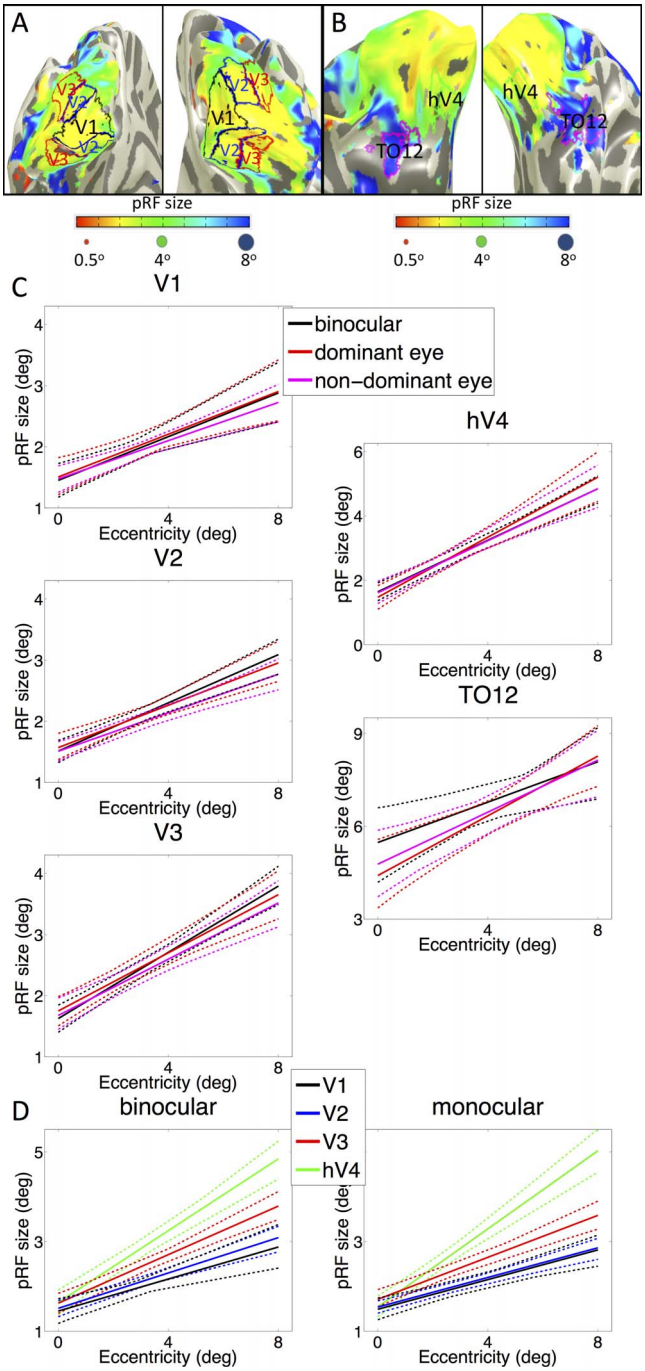

Figure 2. pRF size (σ) as a function of eccentricity. pRF size maps on the cortical surface are shown (**A**) for V1 to V3 and (**B**) hV4 and TO1/TO2. The color bars beneath the maps relate to the pRF sizes. These are the maps of subject 4 (according to the order used in Supplementary Fig. S1), whose maps were selected to be representative of our data. (**C**) pRF size is plotted as a function of eccentricity. Plotted are binocular (*black*), nondominant (*magenta*) and dominant eye (*red*) viewing conditions for areas V1 to V3 (*left*) and hV4 and TO12 (*right*). (**D**) Plots of the pRF sizes in areas V1, V2, V3, and hV4 are also shown, respectively, in the colors *black*, *blue*, *red*, and *green*. *Dotted lines* mark the range of pRF sizes derived from 95% of the observation resulting from 1000 bootstrap samples of baseline fitting.

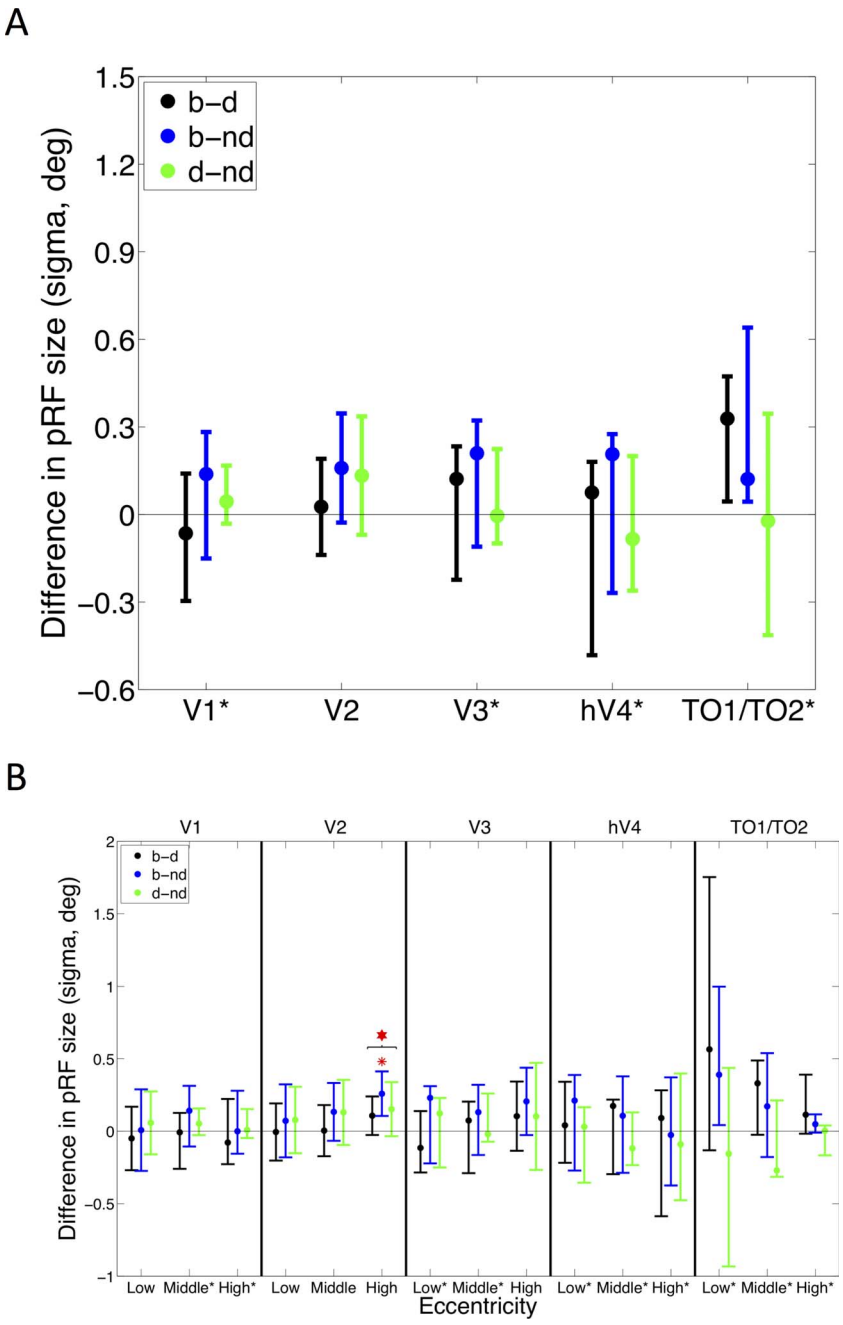

Figure 3. The differences in pRF size among viewing conditions. Shown are the results (**A**) at 4°, and (**B**) at relatively low (0.5°–2.5°), middle (2.5°–5°), and high (5°–7.5°) eccentricities. Differences between binocular and dominant eye (*black*), binocular and nondominant eye (*blue*) and dominant and nondominant eye (*green*) stimulation are presented. On the *x*-axis, labels are marked with a *star* to indicate nonparametric medians and 95% confidence intervals (CIs). For unmarked labels, the parametric means and 95% CIs are shown. Error bars represent the 95% CIs. The *red hexagram* and *star* respectively indicate the only significant ANOVA and post hoc result after multiple comparisons.

comparisons. No differences in amplitude were found between dominant eye and nondominant eye stimulation (Fig. 5A).

Higher binocular than monocular amplitudes were found at 0.5° to 2.5° (V1, V3), 2.5° to 5° (V3) and 5° to 7.5° (V2, V3) eccentricities. Moreover, significant effects were found for the other eccentricity ranges in V1 to V3 but did not pass correction for multiple comparisons. This suggests that higher binocular than monocular amplitudes were consistent across eccentricities (Fig. 5B).

No main effects of order were found for the pRF size nor for the amplitudes analysis.

Binocular Summation

As neither amplitude, nor pRF size differed between dominant and nondominant viewing conditions, average monocular responses were used to calculate binocular summation ratios (Fig. 6). These summation ratios were statistically compared to 1 (zero summation).

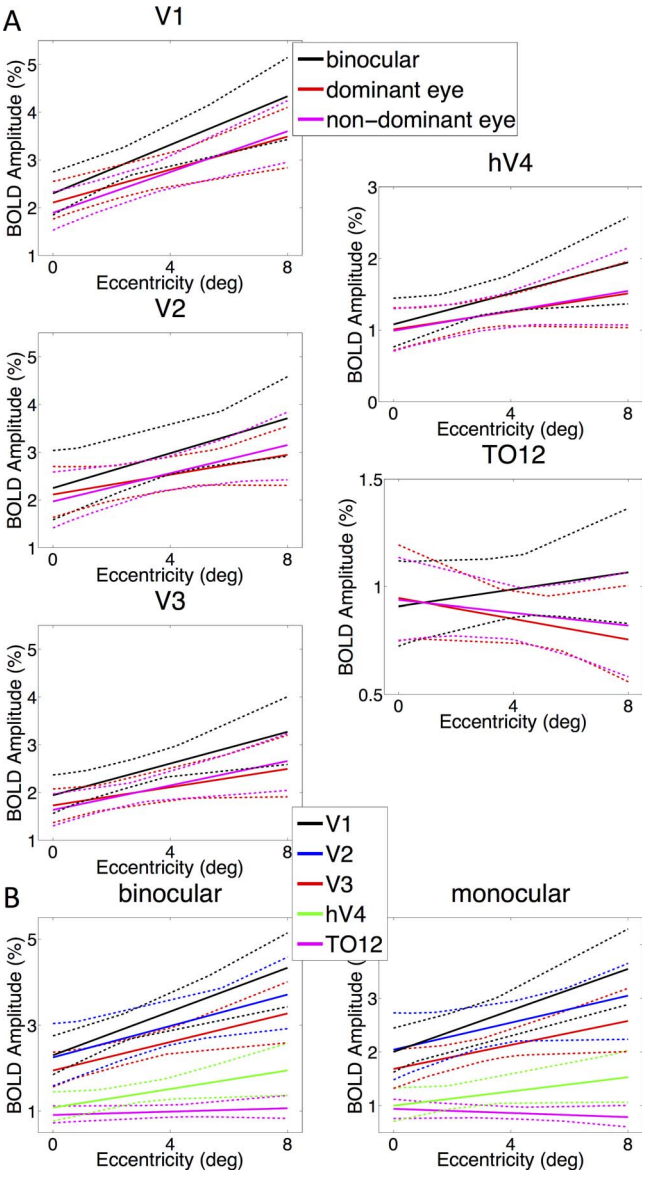

Figure 4. (**A**) BOLD amplitude as a function of eccentricity is plotted for binocular (*black*), nondominant (*magenta*), and dominant eye (*red*) viewing conditions. These are plotted for areas V1 to V3 (*left*) and hV4 and TO12 (*right*). (**B**) Plots of the amplitudes in areas V1 (*black*), V2 (*blue*), V3 (*red*), hV4 (*green*), and TO12 (*magenta*) are shown. *Dotted lines* mark the range of amplitudes derived from 95% of the observation resulting from 1000 bootstrap samples of baseline fitting.

At 4°, there was significant summation for amplitude (Fig. 6A) but not for pRF size (Fig. 6B). Summation in V1–V3 was significant for all eccentricities, except 0.5° to 2.5° in V2, suggesting that amplitude summation consistently occurred across almost all eccentricities in these areas. The pRF size ratio at 5° to 7.5° in V2 was significantly higher than 1 in correspondence to the earlier described difference in pRF size between binocular and nondominant eye stimulation in the same area.

Interindividual and Intervoxel Variability of Amplitude Binocular Summation

An amplitude summation higher than 1, as derived from the average individual binocular and monocular amplitudes, was consistently present among subjects (12 of 13 subjects in V1, hV4, and TO1/TO2, and in 13 of 13 subjects in V2 and V3; see Supplementary Fig. S1a).

Additionally, summation ratios for the individual voxels in each condition along V1 to hV4 were computed. Summation ratios were larger than 1 in high percentages of voxels (Supplementary Fig. S1b).

The consistency of amplitude summation ratios, across subjects and voxels, underlines the robustness of these data despite small participant numbers.

Discussion

Our results suggested that neither the amplitude nor the receptive field size present intereye differences and therefore cannot explain the different roles of the sighting dominant and the nondominant eyes.

Binocular vision, as compared to monocular, resulted in amplitude increase by a factor of approximately 1.2, while in most cases, receptive field sizes were similar, suggesting increased binocular response intensity as the basis for the binocular summation phenomenon.

Despite no clear differences in pRF size, one should keep in mind that small differences may exist but are obscured by data variability or methodological limitations. For the former, our relatively small sample size could have masked differences among conditions, but given the 95% confidence intervals for pRF size, any masked effects must be very subtle. With respect to the methodology used, spatial resolution of the fMRI, limited by voxel size (2.5 mm isotropic), may obscure size effects. However, using the model, we are not looking at the single neuron level but at the population. On that level of resolution, significant differences, if existing, would have emerged.

Negligible Effect of Ocular Dominance on Visual Field Cortical Representation

Sighting ocular dominance describes the dominant eye as the one that defines binocular vision. Unlike handedness, eyedness is known to be a subtle phenomenon, and many people are not aware of the fact that they have a favored eye.[12] The nonrigid nature of ocular dominance, shown by several studies, is therefore not surprising. For example, short periods (several hours) of monocular deprivation were reported to influence the occluded eye's contribution to the binocular percept.[37,38] This plasticity was suggested to result from interocular contralateral inhibitory signals that change following patching.[37,39]

Furthermore, sighting ocular dominance was also reported to be biased by direction of gaze,[12,40] with gazing to the left increasing the prevalence of left eye dominance in individuals with straight-gaze right eye dominance, and vice versa. Thus, if eye dominance is unstable over time and context-dependent, as it appears to be, the probability of finding a stable neural correlate is low.

While several reports suggested sighting eye dominance effects on the size of the activated brain area,[14] VEP latency[41] and amplitude,[42] others reported no such effects (BOLD % signal change[15,16]; VEP amplitude[41]). Similar to our study, a small sample of four subjects (used as a control group) revealed no difference in pRF sizes as a function of sighting ocular dominance.[32]

We thus suggest that this variability among the different studies may reflect differences in experimental design but mainly highlights the context-dependency of ocular dominance.

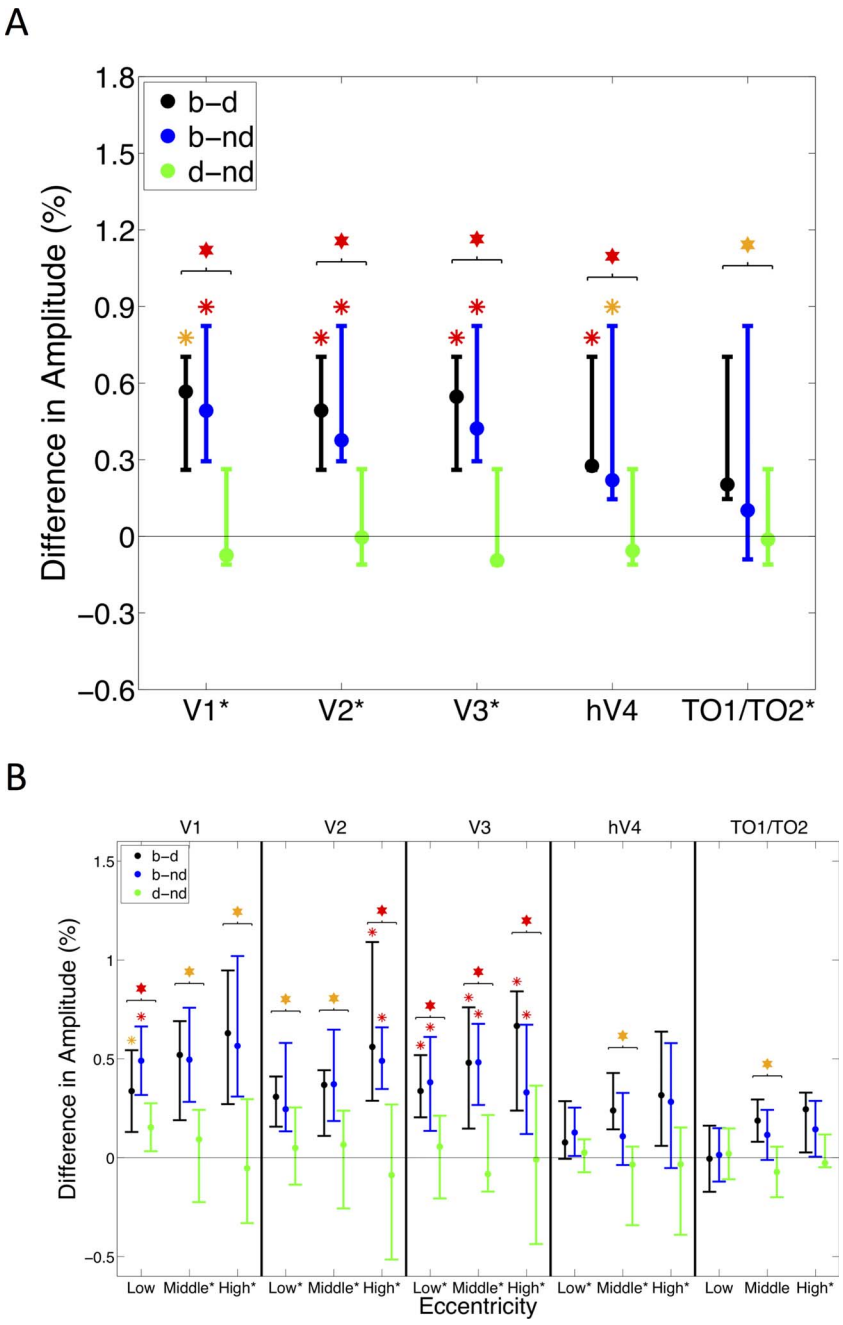

Figure 5. The differences in amplitude among viewing conditions. Shown are the results (**A**) at 4°, and (**B**) relatively low (0.5°–2.5°), middle (2.5°–5°), and high (5°–7.5°) eccentricities. Differences between binocular and dominant eye (*black*), binocular and nondominant eye (*blue*) and dominant and nondominant eye (*green*) stimulation are presented. On the *x*-axis, labels are marked with a star to indicate nonparametric medians and 95% confidence intervals (CIs). For unmarked labels, the parametric means and 95% CIs are shown. Error bars represent the 95% CIs. *Red hexagrams* and *stars* respectively indicate significant ANOVA and post hoc results after multiple comparisons. *Orange hexagrams* and *stars* mark effects that are significant without multiple comparisons.

Similar Binocular and Monocular Receptive Fields' Sizes

Higher binocular compared to nondominant pRF size was found at 5° to 7.5° in V2, suggesting that the binocular pRF size is driven more by the dominant rather than the nondominant eye. However, this effect was quite subtle and did not occur in other areas or at other eccentricities. Assessing the pRF size in a larger participant group could reveal a more general effect, but we suggest that the effect could be considered negligible, relative to potential disease-specific monocular-binocular differences in unilateral eye diseases.

Binocular Summation Seems Derived From Response Amplitude

Our findings of elevated binocular amplitude summation ratios are in line with cats' and monkeys' cellular recordings, demonstrating higher firing rates during binocular versus monocular stimulations.[6–8,13] The complementary similarity

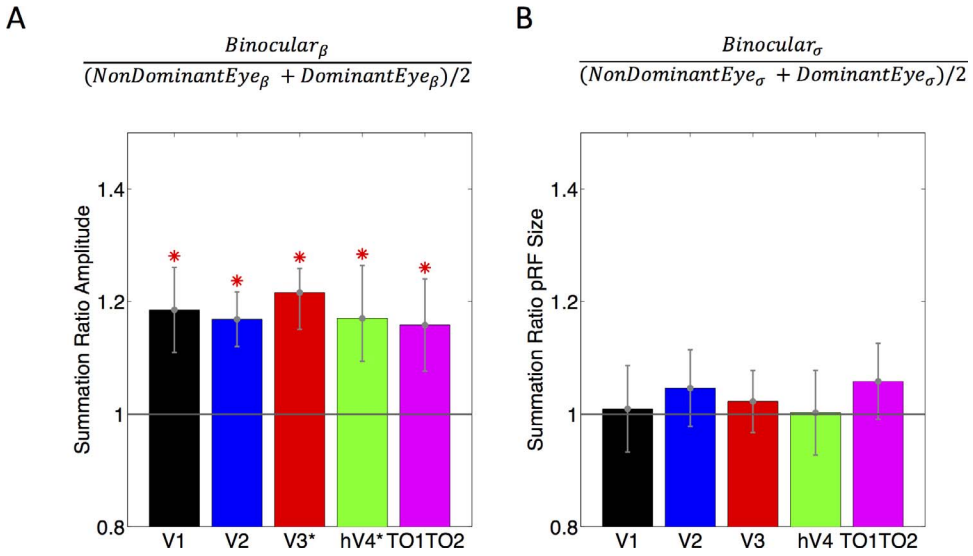

Figure 6. Binocular summation ratios. Amplitude (**A**) and pRF size (**B**) summation ratios represent the 4° outcome-eccentricity baseline fit. Summation ratios' formulas are shown at the top. On the *x*-axis, labels are marked with a *star* to indicate nonparametric medians and 95% confidence intervals (CIs). For unmarked labels, the parametric means and 95% CIs are shown. Error bars represent 95% CIs. *Red stars* mark effects significant after multiple comparisons correction.

between the monocular and binocular receptive field sizes has also been previously described.[43]

Theoretically, summation ratios higher than 1 can reflect performance superiority in binocular compared with monocular conditions, and we consider any such ratios to reflect binocular summation. In psychophysical experiments, it has been proposed that this phenomenon simply stems from "probability summation": presentation of visual inputs to both eyes results in a double chance of producing the correct response.[44] However, binocular contrast summation ratios higher than 1.25 cannot be explained solely by chance[45–47] and should be interpreted as neural interaction summation. Thus, the behavioral binocular summation ratios of 1.42 to 2.0 in foveal regions indicate a neuronal origin.[2,3,45,46] The behavioral phenomenon is influenced by saturation effects[1] in the sense that ratios are reduced with higher stimulus contrast and with longer periods of stimulus presentation but still reflect a real neurological phenomenon.[44,47,48]

In neuronal recording experiments, the measured variable is different, and if monocular inputs are parallel and no neural interactions exist, binocular BOLD peaks and VEP amplitudes should have twice the magnitude of the monocular response.[9] If such is not the case, this would suggest neural interaction summation. More explicitly, higher ratios may indicate synergistic, while lower values inhibitory, interactions.

In reality, our binocular inputs fuse into a cyclopean world representation, which enables, for example, stable contrast perception that occurs whether we look at an image with one or two eyes.[9,49] Thus, previously found summation ratios other than 2 in EEG VEP amplitudes (i.e., 1.26–2.1[50–52]) and in an fMRI study (at low contrast; i.e., 1.55[9]) are in line with the phenomenon of neural summation. Binocular summation ratios were higher in response to binocular stimuli with perpendicular orientations than to binocular stimuli with identical orientations, suggesting that the interocular suppression involved in the binocular neural interactions is orientation-specific.[9]

Interestingly, a recent study revealed binocular summation to differently affect the different components of the VEP (summation ratios of 1.5–1.7 for the N75; 1.2–1.3 for the P100; and 1.4 for the N145).[53] Latencies were unaffected.[53] Based on cortical sourcing, we know that N75 originates solely from V1 sources, while P100 also has extra-striate sources.[54–59] This would seem to imply that along the visual hierarchy, binocular summation is initially robust and later inhibited.

Additionally, a combined electrocorticography (ECoG) and fMRI study revealed that the ECoG signal has two components, that is, a stimulus-locked, linear component and an asynchronous, broadband component.[60] When both components and the fMRI BOLD signal were pRF modeled, it was found that the stimulus-locked pRF reflected linear spatial summation, possibly originating from the input layers (4C) of the visual cortex.[60] The fMRI and broadband ECoG component pRFs were analogous, reflecting highly similar sublinear summation, probably originating from layers 2 and 3. These pRFs would reflect later stages of the visual processing,[60] suggesting that the binocular summation ratio of 1.2 also reflects later visual processing stages.

Therefore, it seems that the different summation ratios reported in the literature reflect different stages of visual processing along the visual hierarchy.

What Are Possible Behavioral Roles of High-Contrast Binocular Summations?

We have discussed roles of binocular summation in 2-dimensional vision. Another possible advantage for binocular summation is its role in depth perception. Support for this relationship can be found in the fact that binocular summation appears strongest at zero disparity and decreases with increasing binocular disparity.[61] Increased binocular summation was also found to be associated with improved stereoacuity after strabismus surgery.[62] Reduced VEP and reduced contrast binocular summation have also been found in stereo-impaired individuals.[63,64] Moreover, whereas binocular summation is stronger at low contrasts,[1] sensitivity to binocular disparity rises with increasing contrast.[65] Binocular summation has also been found to facilitate actions such as reflexive eye movements and even walking.[66,67]

Limitations

An important limitation of our study is the low number of subjects. Still, as discussed above, amplitude summation was consistently present in all subjects and across voxels, suggesting that our low sample size is unlikely to bias results.

Additionally, the fixation control task (previously used by Dumoulin and Wandell,[18] Harvey and Dumoulin,[19] Zuiderbaan et al.,[26] Amano et al.,[30] and Clavagnier et al.[32]) is not very demanding and thus attentional effects could influence our results.[68–70] However, in light of the ocular dominance context-dependency on which we previously elaborated, we do not rule out the possibility that attention plays a role in the studied phenomena.

Another concern that should be raised is the effect of disparity. For a flat display, a single stimulus gives rise to two different images in the two eyes, and this effect is accentuated at high eccentricities. As a result, binocular stimulation might give rise to different pRF sizes (compared to monocular viewing) simply due to different retinal images. To that end, we want to emphasize that zero-disparity horopter closely corresponds to a flat screen until eccentricities of up to 10 degrees[71] and our stimuli were limited to 8 degrees. Thus, binocular disparity effects that may occur due to increases in eccentricity are negligible in our case.

Conclusions and Future Directions

It can be concluded that only minor differences exist between binocular and monocular vision with regard to pRF size and that binocularity is mainly reflected by higher binocular amplitudes. There was no effect of ocular dominance on the visual field cortical representation. It would be interesting to further study these effects via ocular dominance columns using ultra-high-field MRIs.

Our results should find application in imaging studies of monocular disease, such as optic neuritis. Optic neuritis is a monocular demyelinating disease of the optic nerve causing acute visual loss and is frequently the presenting symptom of multiple sclerosis.[72–74] Weeks following the acute attack, the amplitudes of the input transmission via the affected eye resolve, but conduction latencies via this side often remain substantially prolonged.[73–75] This prolongation may persist for years following the attack causing intereye temporal mismatch in input arrival to the cortex.[73–75] We have previously suggested a new type of cortical reorganization in recovered optic neuritis patients that would compensate for this unilateral peripheral delay.[75] This adaptation within the temporal domain enables intereye synchronization, and facilitates binocular functions, such as stereopsis perception. Quantifying monocular and binocular field sizes and evaluating their correlation to patients' binocular visual abilities could help us understand the mechanisms of this hypothesized reorganization process.

Acknowledgments

The authors thank Atira Bick for her valuable statistical advice.

Supported by the European Union's Horizon 2020 research and innovation program under the Marie Sklodowska-Curie Grant agreement No. 641805, and the National MS Society Research Grant 5128-A-1.

Disclosure: **P.B. de Best**, None; **N. Raz**, None; **S. Dumoulin**, None; **N. Levin**, None

References

1. Bearse MA, Freeman RD. Binocular summation in orientation discrimination depends on stimulus contrast and duration. *Vision Res*. 1994;34:19–29.
2. Grigsby SS, Tsou BH. Grating and flicker sensitivity in the near and far periphery: naso-temporal asymmetries and binocular summation. *Vision Res*. 1994;34:2841–2848.
3. Campbell FW, Green DG. Monocular versus binocular visual acuity. *Nature*. 1965;208:191–192.
4. Legge GE. Binocular contrast summation-I. Detection and discrimination. *Vision Res*. 1984;24:373–383.
5. Wood JM, Collins MJ, Carkeet A. Regional variations in binocular summation across the visual field. *Ophthalmic Physiol Opt*. 1992;12:46–51.
6. Hubel DH, Wiesel TN. Stereoscopic vision in macaque monkey: cells sensitive to binocular depth in area 18 of the macaque monkey cortex. *Nature*. 1970;225:41–42.
7. Hubel DH, Wiesel TN. Receptive fields, binocular interaction and functional architecture in the cat's visual cortex. *J Physiol (Lond)*. 1962;160:106–154.
8. Hubel DH, Wiesel TN. Receptive fields of single neurones in the cat's striate cortex. *J Physiol (Lond)*. 1959;148:574–591.
9. Moradi F, Heeger DJ. Inter-ocular contrast normalization in human visual cortex. *J Vis*. 2009;9(3):13.
10. Mapp AP, Ono H, Barbeito R. What does the dominant eye dominate? A brief and somewhat contentious review. *Percept Psychophys*. 2003;65:310–317.
11. Coren S, Kaplan CP. Patterns of ocular dominance. *Optom Vis Sci*. 1973;50:283–292.
12. Carey DP. Vision research: losing sight of eye dominance. *Curr Biol*. 2001;11:R828–R830.
13. Hubel DH, Wiesel TN, LeVay S. Functional architecture of area 17 in normal and monocularly deprived macaque monkeys. *Cold Spring Harb Symp Quant Biol*. 1976;40:581–589.
14. Rombouts SARB, Barkhof F, Sprenger M, Valk J, Scheltens P. The functional basis of ocular dominance: functional MRI (fMRI) findings. *Neurosci Lett*. 1996;221:1–4.
15. Mendola JD, Conner IP. Eye dominance predicts fMRI signals in human retinotopic cortex. *Neurosci Lett*. 2007;414:30–34.
16. Levin N, Orlov T, Dotan S, Zohary E. Normal and abnormal fMRI activation patterns in the visual cortex after recovery from optic neuritis. *Neuroimage*. 2006;33:1161–1168.
17. Baba M, Sasaki KS, Ohzawa I. Integration of multiple spatial frequency channels in disparity-sensitive neurons in the primary visual cortex. *J Neurosci*. 2015;35:10025–10038.
18. Dumoulin SO, Wandell BA. Population receptive field estimates in human visual cortex. *Neuroimage*. 2008;39:647–660.
19. Harvey BM, Dumoulin SO. The relationship between cortical magnification factor and population receptive field size in human visual cortex: constancies in cortical architecture. *J Neurosci*. 2011;31:13604–13612.
20. Hess R, Field D. Integration of contours: new insights. *Trends Cogn Sci*. 1999;3:480–486.
21. Hupe JM, James AC, Girard P, Lomber SG, Payne BR, Bullier J. Feedback connections act on the early part of the responses in monkey visual cortex. *J Neurophysiol*. 2001;85:134–145.
22. McGraw PV, Whitaker D, Skillen J, Chung STL. Motion adaptation distorts perceived visual position. *Curr Biol*. 2002;12:2042–2047.
23. Tootell RBH, Hadjikhani NK, Mendola JD, Marrett S, Dale AM. From retinotopy to recognition: fMRI in human visual cortex. *Trends Cogn Sci*. 1998;2:174–183.
24. Lou L. Troxler effect with dichoptic stimulus presentations: evidence for binocular inhibitory summation and interocular suppression. *Vision Res*. 2008;48:1514–1521.

25. Klein BP, Harvey BM, Dumoulin SO. Attraction of position preference by spatial attention throughout human visual cortex. *Neuron*. 2014;84:227–237.
26. Zuiderbaan W, Harvey BM, Dumoulin SO. Modeling center-surround configurations in population receptive fields using fMRI. *J Vis*. 2012;12(3):10.
27. Brainard DH. The psychophysics toolbox. *Spat Vis*. 1997;10:433–436.
28. Nestares O, Heeger DJ. Robust multiresolution alignment of MRI brain volumes. *Magn Reson Med*. 2000;43:705–715.
29. Dale AM, Fischl B, Sereno MI. Cortical surface-based analysis: I. Segmentation and surface reconstruction. *Neuroimage*. 1999;9:179–194.
30. Amano K, Wandell BA, Dumoulin SO. Visual field maps, population receptive field sizes, and visual field coverage in the human MT+ complex. *J Neurophysiol*. 2009;102:2704–2718.
31. Witthoft N, Nguyen ML, Golarai G, et al. Where is human V4? Predicting the location of hV4 and VO1 from cortical folding. *Cereb Cortex*. 2013;24:2401–2408.
32. Clavagnier S, Dumoulin SO, Hess RF. Is the cortical deficit in amblyopia due to reduced cortical magnification, loss of neural resolution, or neural disorganization? *J Neurosci*. 2015;35:14740–14755.
33. Field A, Miles J, Field Z. 14.9 Robust analysis of mixed designs. In: *Discovering Statistics Using R*. 1st ed. Thousand Oaks, CA: Sage; 2012:955–964.
34. Mair P, Wilcox RR. *Robust Statistical Methods in R Using the WRS2 Package* [technical report]. Harvard University, 2016. Available at: https://dornsife.usc.edu/assets/sites/239/docs/WRS2.pdf. Accessed October 22, 2018.
35. Wilcox RR. Comparing multiple dependent groups. In: *Introduction to Robust Estimation and Hypothesis Testing*. Amsterdam, The Netherlands: Elsevier; 2011:333–382.
36. Wilcox RR. Comparing two groups. In: *Introduction to Robust Estimation and Hypothesis Testing*. Amsterdam, The Netherlands: Elsevier; 2011:137–202.
37. Spiegel DP, Baldwin AS, Hess RF. Ocular dominance plasticity: inhibitory interactions and contrast equivalence. *Sci Rep*. 2017;7:39913.
38. Zhou J, Clavagnier S, Hess RF. Short-term monocular deprivation strengthens the patched eye's contribution to binocular combination. *J Vis*. 2013;13(5):12.
39. Meese TS, Georgeson MA, Baker DH. Binocular contrast vision at and above threshold. *J Vis*. 2006;6(11):7.
40. Khan AZ, Crawford JD. Ocular dominance reverses as a function of horizontal gaze angle. *Vision Res*. 2001;41:1743–1748.
41. Taghavy A, Kügler CFA. Pattern reversal visual evoked potentials (white-black-and colour-black-PVEPs) in the study of eye dominance. *Eur Arch Psychiatry Clin Neurosci*. 1987;236:329–332.
42. Seyal M, Sato S, White BG, Porter RJ. Visual evoked potentials and eye dominance. *Electroencephalogr Clin Neurophysiol*. 1981;52:424–428.
43. Sanada TM, Ohzawa I. Encoding of three-dimensional surface slant in cat visual areas 17 and 18. *J Neurophysiol*. 2006;95:2768–2786.
44. Blake R, Fox R. The psychophysical inquiry into binocular summation. *Atten Percept Psychophys*. 1973;14:161–185.
45. Baker DH, Meese TS, Mansouri B, Hess RF. Binocular summation of contrast remains intact in strabismic amblyopia. *Invest Ophthalmol Vis Sci*. 2007;48:5332–5338.
46. Gilchrist J, Pardhan S. Binocular contrast detection with unequal monocular illuminance. *Ophthalmic Physiol Opt*. 1987;7:373–377.
47. Cogan AI. Human binocular interaction: towards a neural model. *Vision Res*. 1987;27:2125–2139.
48. Fry GA, Bartley SH. The brilliance of an object seen binocularly. *Am J Ophthalmol*. 1933;16:687–693.
49. Barendregt M, Harvey BM, Rokers B, Dumoulin SO. Transformation from a retinal to a cyclopean representation in human visual cortex. *Curr Biol*. 2015;25:1982–1987.
50. Heravian JS, Jenkins TCA, Douthwaite WA. Binocular summation in visually evoked responses and visual acuity. *Ophthalmic Physiol Opt*. 1990;10:257–261.
51. Lefebvre L, Theoret H, Saint-Amour D. A novel way to make transient-VEPs a better predictor of human binocular integration. *Neuroreport*. 2010;21:1023–1028.
52. Plainis S, Petratou D, Giannakopoulou T, Atchison DA, Tsilimbaris MK. Binocular summation improves performance to defocus-induced blur. *Invest Ophthalmol Vis Sci*. 2011;52:2784–2789.
53. Czainska M, Przekoracha-Krawczyk AN, Naskrecki R, van der Lubbe RO. Binocular summation evaluated by early and late visual evoked potentials. *Optica Applicata*. 2018;48:137–148.
54. Martínez A, Di Russo F, Anllo-Vento L, Sereno MI, Buxton RB, Hillyard SA. Putting spatial attention on the map: timing and localization of stimulus selection processes in striate and extrastriate visual areas. *Vision Res*. 2001;41:1437–1457.
55. Ossenblok P, Spekreijse H. The extrastriate generators of the EP to checkerboard onset. A source localization approach. *Electroencephalogr Clin Neurophysiol*. 1991;80:181–193.
56. Maier J, Dagnelie G, Spekreijse H, van Dijk BW. Principal components analysis for source localization of VEPs in man. *Vision Res*. 1987;27:165–177.
57. Di Russo F, Pitzalis S, Spitoni G, et al. Identification of the neural sources of the pattern-reversal VEP. *Neuroimage*. 2005;24:874–886.
58. Martínez A, Anllo-Vento L, Sereno MI, et al. Involvement of striate and extrastriate visual cortical areas in spatial attention. *Nat Neurosci*. 1999;2:364–369.
59. Clark VP, Hillyard SA. Spatial selective attention affects early extrastriate but not striate components of the visual evoked potential. *J Cogn Neurosci*. 1996;8:387–402.
60. Winawer J, Kay KN, Foster BL, Rauschecker AM, Parvizi J, Wandell BA. Asynchronous broadband signals are the principal source of the BOLD response in human visual cortex. *Curr Biol*. 2013;23:1145–1153.
61. Rose D, Blake R, Halpern DL. Disparity range for binocular summation. *Invest Ophthalmol Vis Sci*. 1988;29:283–290.
62. Kattan JM, Velez FG, Demer JL, Pineles SL. Relationship between binocular summation and stereoacuity after strabismus surgery. *Am J Ophthalmol*. 2016;165:29–32.
63. Lema SA, Blake R. Binocular summation in normal and stereoblind humans. *Vision Res*. 1977;17:691–695.
64. Amigo G, Fiorentini A, Pirchio M, Spinelli D. Binocular vision tested with visual evoked potentials in children and infants. *Invest Ophthalmol Vis Sci*. 1978;17:910–915.
65. Halpern DL, Blake RR. How contrast affects stereoacuity. *Perception*. 1988;17:483–495.
66. Quaia C, Optican LM, Cumming BG. Binocular summation for reflexive eye movements. *J Vis*. 2018;18(4):7.
67. Hayhoe M, Gillam B, Chajka K, Vecellio E. The role of binocular vision in walking. *Vis Neurosci*. 2009;26:73–80.
68. Burtis DB, Williamson JB, Mishra M, Heilman KM. The blindside: impact of monocular occlusion on spatial attention. *J Clin Exp Neuropsychol*. 2013;35:291–297.
69. Chen P, Erdahl L, Barrett AM. Monocular patching may induce ipsilateral "where" spatial bias. *Neuropsychologia*. 2009;47:711–716.

Investigative Ophthalmology & Visual Science

70. Roth HL, Lora AN, Heilman KM. Effects of monocular viewing and eye dominance on spatial attention. *Brain*. 2002;125: 2023–2035.
71. Ciuffreda KJ, Engber K. Is one eye better than two when viewing pictorial art? *Leonardo*. 2002;35:37–40.
72. Halliday AM, McDonald WI, Mushin J. Delayed visual evoked response in optic neuritis. *Lancet*. 1972;299:982–985.
73. Raz N, Dotan S, Benoliel T, Chokron S, Ben-Hur T, Levin N. Sustained motion perception deficit following optic neuritis: behavioral and cortical evidence. *Neurology*. 2011;76:2103–2111.
74. Raz N, Dotan S, Chokron S, Ben-Hur T, Levin N. Demyelination affects temporal aspects of perception: an optic neuritis study. *Ann Neurol*. 2012;71:531–538.
75. Raz N, Chokron S, Ben-Hur T, Levin N. Temporal reorganization to overcome monocular demyelination. *Neurology*. 2013; 81:702–709.

Investigative Ophthalmology & Visual Science